NANO LETTERS

Letter

pubs.acs.org/NanoLett

Nitride Stabilized PtNi Core–Shell Nanocatalyst for high Oxygen Reduction Activity

Kurian A. Kuttiyiel,[†] Kotaro Sasaki,[†] YongMan Choi,[†,§] Dong Su,[‡] Ping Liu,[†] and Radoslav R. Adzic*[,†]

[†]Chemistry Department, Brookhaven National Laboratory, Upton, New York 11973, United States

[‡]Center for Functional Nanomaterials, Brookhaven National Laboratory, Upton, New York 11973, United States

[§]Chemical Catalysis, SABIC Technology Center, Riyadh, 11551, Saudi Arabia

Supporting Information

ABSTRACT: We describe a route to the development of novel PtNiN core–shell catalysts with low Pt content shell and inexpensive NiN core having high activity and stability for the oxygen reduction reaction (ORR). The PtNiN synthesis involves nitriding Ni nanoparticles and simultaneously encapsulating it by 2–4 monolayer-thick Pt shell. The experimental data and the density functional theory calculations indicate nitride has the bifunctional effect that facilitates formation of the core–shell structures and improves the performance of the Pt shell by inducing both geometric and electronic effects. Synthesis of inexpensive NiN cores opens up possibilities for designing of various transition metal nitride based core–shell nanoparticles for a wide range of applications in energy conversion processes.

KEYWORDS: *Electrocatalysis, core–shell nanoparticles, oxygen reduction reaction, nickel nitride, catalyst stability, fuel cells*

In polymer electrolyte membrane fuel cells (PEMFCs), the oxygen reduction reaction (ORR) electrode catalyst material of choice has been platinum (Pt) for decades.[1,2] However, the ORR on Pt is irreversible, thus causing overpotentials and losses in fuel cell efficiency.[3−5] Recent efforts have been devoted toward optimization and design new catalysts with minimum usage of Pt which include concepts like alloying metals,[6,7] the Pt monolayer approach[8−10] and dealloying method.[11−13] These studies have led each to specific improvements to catalyst performance, but large increase in activity, controlled large-scale synthesis and durability still remains a challenge.[14,15] Although multiple mechanisms has been proposed to explain the high ORR activity of platinum–nickel (PtNi) structures,[16−18] these catalysts have high Pt content and also lack durability as harsh oxidation conditions lead to their loss of structural integrity,[19,20] encumbering the development of highly active, stable and low cost cathode materials. Indeed, these limitations could be challenged by substantially decreasing the Pt loading and increasing its stability using core–shell nanostructures.[21−24]

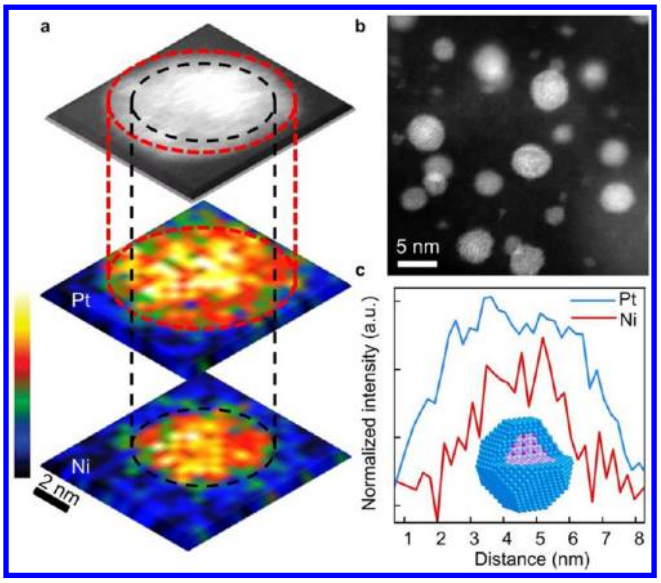

Figure 1. (a) HAADF-STEM image of a PtNiN core–shell nanoparticle with its corresponding two-dimensional EELS mapping of Pt M and Ni L signals. (dotted lines for visualization purpose only). (b) STEM image of PtNiN core–shell nanoparticles. (c) EELS line-scan profiles of Pt and Ni in a single nanoparticle along with schematic representation of a single PtNiN nanoparticle. (blue, Pt; gray, Ni; purple, N).

Here, we report the structure and the performance of well-defined core–shell nanoparticles consisting of Pt shell on Ni nitride core. Owing to it having one of the strongest covalent bonds, nitrogen (N) is very stable and inert under normal conditions. Yet nitrogen reacts with selected elements, forming compounds with a variety of intriguing properties. Although transition metal nitrides are known for their electrochemical

Received: September 9, 2012
Revised: October 26, 2012
Published: November 29, 2012

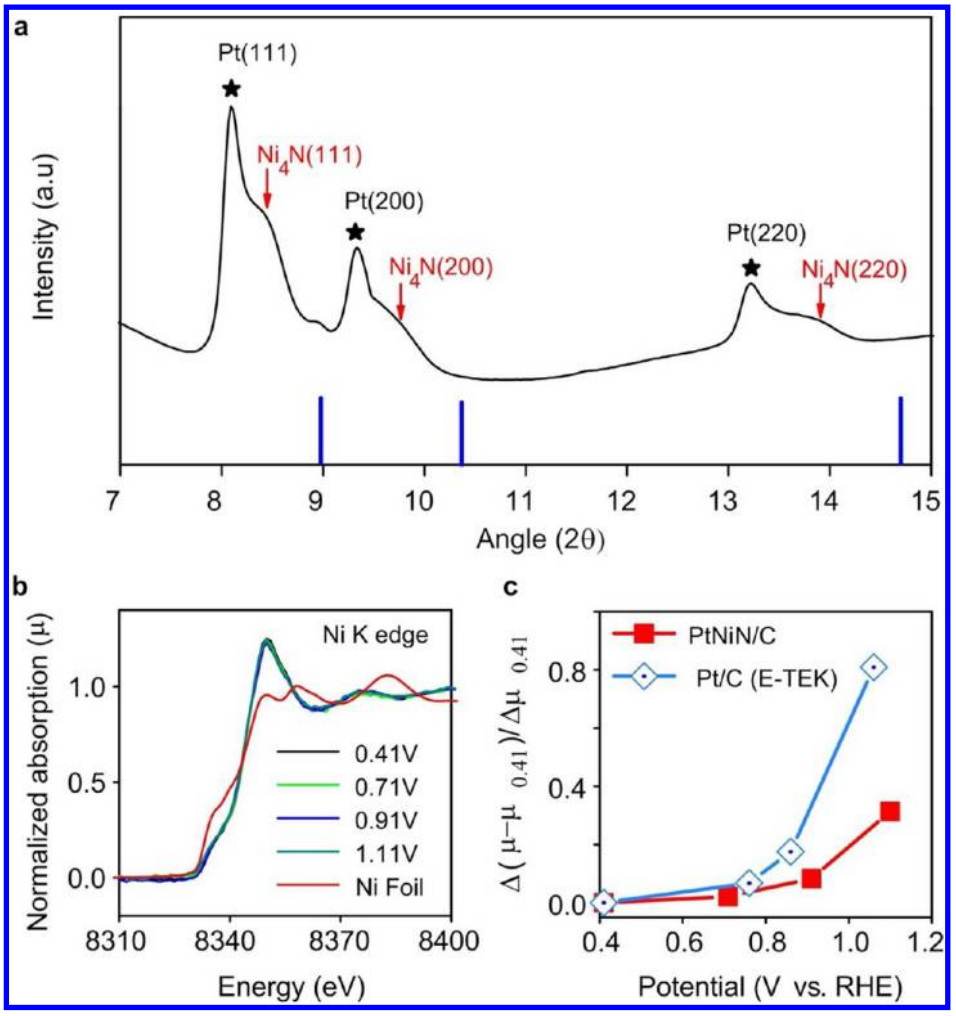

Figure 2. (a) Synchrotron XRD pattern for PtNiN catalyst showing Pt and Ni_4N phases. (blue line denotes Ni_3N phase). (b) In situ XANES of Ni K edge for PtNiN electrocatalyst at various potentials. (c) Comparison of the change of the Pt adsorption edge peaks of the XANES spectra for PtNiN/C and Pt/C as a function of potential obtained in 1 M $HClO_4$.

stability, they lack the desired catalytic activity so as to be used as PEMFC catalyst.[25,26] We demonstrate that using a low content of Pt and NH_3 as a reactive environment, PtNi nanoparticles can undergo profound structural and chemical changes forming Ni_4N in the core and thin Pt layer as shell. Using density functional theory (DFT) calculations, we investigate the role of N atoms in the core−shell structured catalyst. The N and the core−shell structure in the PtNiN core−shell nanoparticles increases the Pt ORR activity and provide a stabilizing effect under high oxidizing conditions suppressing the dissolution during potential cycling.

PtNiN core−shell nanoparticles were synthesized by chemical reduction (see methods) and subsequent thermal annealing in N_2 followed by using NH_3 as nitrogen precursor at ambient pressure. The nanoparticles obtained were nearly sphere-like shape and had an average diameter of 3.5 nm (Figure S1, Supporting Information). Physical characterization of the nanoparticles was performed by electron energy-loss spectroscopy (EELS) mapping for Pt M (2122 eV) and Ni L (855 eV) edges using a scanning transmission electron microscope (STEM) equipped with aberration-correction system. The high angle annular dark-field (HAADF) image (Figure 1), whose contrast is directly related to atomic number Z, reveals the core−shell structure of the nanoparticles. Overlapping the two-dimensional mapping of Pt and Ni EELS signal from a single nanoparticle as shown in Figure 1a (dotted lines) validates the core−shell structure. The EELS line scan profile indicates the distribution of Pt and Ni components in a representative single nanoparticle, where the Pt shell thickness can be directly measured (Figure 1c). The Pt shell thickness measured on various nanoparticles was around 0.5 to 1.0 nm, equivalent to 2 to 4 monolayers of Pt on the Ni rich core. The overall weight percentage of Pt and Ni in the carbon supported PtNiN core−shell nanoparticles was 10.2% and 3.5% respectively which accounts to a molar ratio of 1, as determined by inductively coupled plasma optical emission spectrometry (ICP-OES) measurements.

The core−shell nanoparticles were further characterized using synchrotron X-ray diffraction (XRD) which suggests the formation of nickel-nitride (NiN) compound. The diffraction pattern of the as prepared core−shell nanoparticles (Figure 2a) exhibits only the reflections of Pt and Ni_4N that has the structure of primitive cubic lattice. The pattern points to the formation of a PtNi solid-solution alloy with an average size of 3.6 nm estimated from the Scherer's equation. Another intriguing feature is that peaks ascribed to reflections from (200) and (220) of the Ni metal phase are missing, indicating that the catalyst contains mostly NiN phases. A relatively

dx.doi.org/10.1021/nl303362s | Nano Lett. 2012, 12, 6266−6271

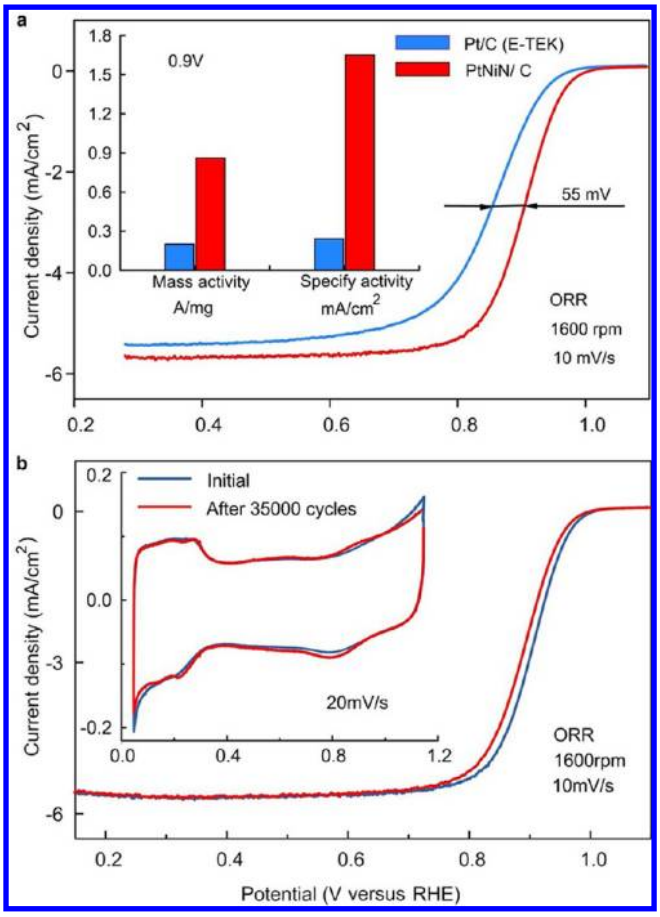

Figure 3. (a) Polarization curves for ORR and (inset) mass and specific activities for PtNiN/C and Pt/C catalysts on a RDE electrode. Pt loading for PtNiN/C and Pt/C were 7.84 and 7.65 $\mu g/cm^2$ respectively. (b) ORR polarization and voltammetry (inset) curves of PtNiN core−shell nanoparticles before and after 35000 cycle test between 0.6 and 1.05 V in 0.1 M $HClO_4$.

smaller peak appearing at 8.98° may correspond to a Ni_3N or Ni metal phase as the literature confirms that both phases have (111) reflections at the same 2θ value.[27,28] To clarify the absences of Ni metal, we analyzed the XRD pattern of the PtNi nanoparticles annealed at 250 °C in N_2 (before NH_3 treatment). PtNi forms a solid solution alloy when annealed at 250 °C in N_2 without showing any discrete peaks for Ni (Figure S2, Supporting Information). The Ni_3N (111) phase appears only after the catalyst undergoes the NH_3 treatment. This clearly justifies that some of the Ni_4N phases is decomposed to Ni_3N phases which might happen when the sample is cooled down to room temperature in NH_3 environment, as Ni_3N is formed at temperatures between 200 and 350 °C.[29] Moreover the inclusion of N in the PtNi nanoparticles pushes the Pt (111) peak to higher angles (Figure S2, Supporting Information) and an increase line broadening was also observed indicating a distortion of the lattice due to N atoms. This change in the lattice structure is due to the chemical interaction of metal atoms with N, resulting in the formation of nitrides.[29,30] Thus, synchrotron XRD confirms that Ni in the PtNiN core−shell nanoparticles is nitrided forming Ni_4N species.

The stabilizing effect of the core−shell structure for PtNiN nanoparticles was determined by in situ X-ray absorption near edge spectroscopy (XANES) (Figure 2b). In situ XANES of the Ni K edges from the PtNiN nanoparticles in 1 M $HClO_4$, together with reference material, viz., Ni foil (thickness ≈10 μm) suggest that electronic properties of Ni have been changed by alloying with N and Pt. Also no changes in energy were observed at various potential of 0.41−1.11 V, signifying that the Pt shell is protecting the Ni core from oxidation. The XANES data for Pt L_3 edges offer strong evidence of decreased oxidation of Pt in PtNiN nanoparticles in comparison with commercially available Pt nanoparticles (Figures 2c and S4, Supporting Information). The high Pt oxidation potential (lower extent of Pt oxidation) of PtNiN catalyst clearly suggests the interaction of the underlying metal via geometric and electronic effects.[11,12] A decreased Pt oxidation can also be observed from the comparison of voltammetry curves for PtNiN/C and Pt/C catalyst (Figure S3, Supporting Information).

The electrocatalytic activity of carbon supported PtNiN core−shell nanoparticles toward the ORR was benchmarked against the commercially available Pt/C catalyst (E-TEK, 10% wt. of 3.2 nm Pt nanoparticles on Vulcan XC-72 carbon support). The cyclic voltammetry (CV) curves for PtNiN catalysts (Figure S3, Supporting Information), recorded at room temperature in Ar-purged 0.1 M $HClO_4$ solution, did not show any anodic currents ascribed to the oxidation/dissolution of Ni, demonstrating that Ni is protected by the Pt shell. The half wave potential measured from the ORR polarization curves at 1600 rpm (Figure 3) for PtNiN core−shell catalyst was 905 mV which was 55 mV higher than pure Pt/C catalyst. The kinetic current was calculated from the ORR polarization curves by using the Koutecky−Levich equation at various rpm in O_2-purged 0.1 M $HClO_4$ solution at a sweep rate of 10 mV/s. To calculate the mass activity, the kinetic current was normalized to the loading amount of Pt and to compare specific activity the current was normalized to the electrochemically active surface area (ECSA) calculated by measuring the charge collected in the H_{upd} adsorption/desorption region after double-layer correction and assuming a value of 210 $\mu C/cm^2$ for the adsorption of a hydrogen monolayer.[31] At room temperature, the PtNiN catalyst exhibited mass and specific activities of 0.86 A/mg_{Pt} and 1.65 mA/cm^2 respectively at 0.9 V versus a reversible hydrogen electrode (RHE) that were both around 4.5 to 6.5 times greater than that of the Pt/C (0.20 A/mg_{Pt} and 0.24 mA/cm^2).

We also performed accelerated durability tests by applying linear potential sweeps between 0.6 and 1.05 V at 50 mV/s in air-saturated 0.1 M $HClO_4$ solution at room temperature. After 35000 cycles, the CV measurements showed no loss in ECSA for the PtNiN core−shell electrocatalyst (Figure 3b). In contrast with Pt/C that has been demonstrated to lose almost 45% of its initial area,[32] the PtNiN core−shell electrocatalyst has much better resilience under high oxidizing conditions. To measure the ORR degradation after cycling we compared the initial and final half wave potentials at 1600 rpm in O_2 saturated 0.1 M $HClO_4$ solution. After 35000 cycles the ORR measurements showed only 11 mV loss in its half wave potential, suggesting PtNiN catalyst has a very good stability for the ORR. We used STEM-EELS analyses to examine the structure of the PtNiN core−shell nanoparticles after potential cycling to elucidate the questions about Ni leaching out in harsh acid environment (Figures 4 and S5, Supporting Information). The overlapping of the Ni EELS (red) and Pt signal (blue) of a single representative nanoparticle (Figure 4, parts a and b) after 35000 potential cycles clearly shows that

dx.doi.org/10.1021/nl303362s | Nano Lett. 2012, 12, 6266−6271

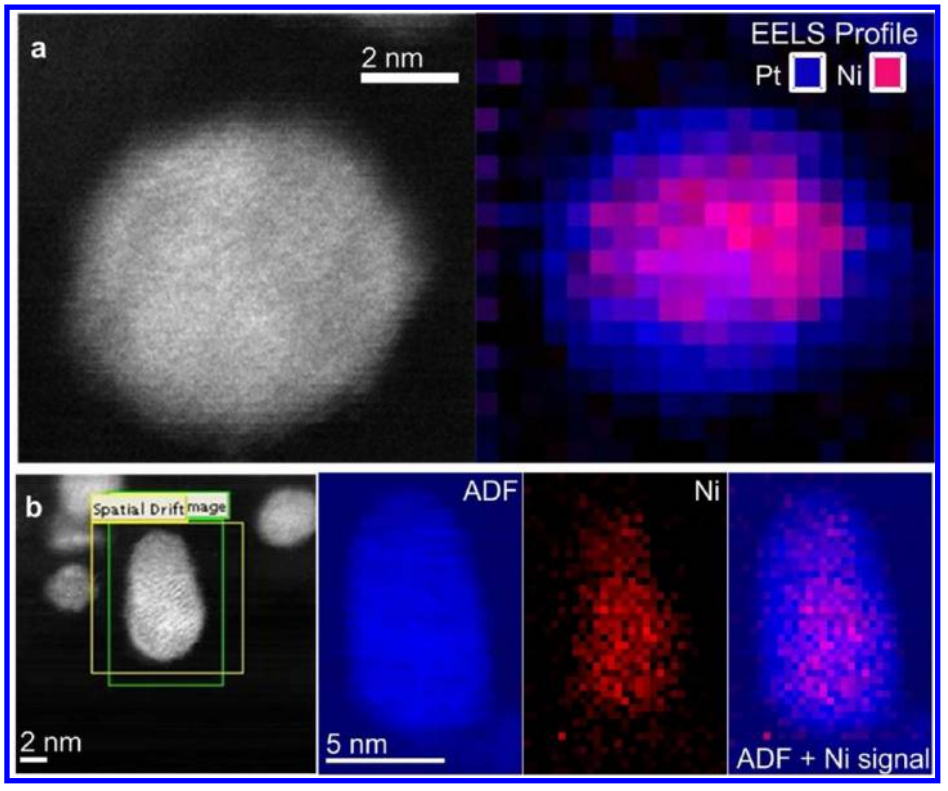

Figure 4. (a and b) HAADF image of representative nanoparticles after potential cycling along with its respective 2-D EELS mapping of Pt M edge (blue) and Ni L edge(red).

the core−shell structure of the PtNiN nanoparticle is intact further attesting the performance durability of the catalyst.

To elucidate the enhanced ORR activity and durability of PtNiN/C compared to those of Pt/C, we carried out density functional theory (DFT) calculations using a sphere-like nanoparticle model with ∼1.7 nm (Figure S6, Supporting Information). To simulate the experimental finding of the Ni_4N of the core material (Figure 2), we kept the mole ratio of Ni and N approximately 20% by using the bulk Ni_4N structure ($a_{0,\ DFT}$ = 3.756 Å) and to save computational time we used only two Pt layers for modeling the Pt shell, consisting of 182 Pt, 19 Ni, and 4 N atoms ($Pt_{2ML}Ni_4N$). As shown in Figure S7 and Table S1, Supporting Information, we calculated the surface strain, the d-band center of Pt in the shell, and the binding energy of oxygen (BE-O) as a descriptor for the ORR activity.[33] Similar to the previous study,[8] an oxygen atom was placed at a fcc active site on the nanoparticle to calculate BE-Os (Figure S6, Supporting Information). The results show that $Pt_{2ML}Ni_4N$ and $Pt_{2ML}Ni$ (two monolayers of the Pt shell on a Ni core) behave more likely to pure Pt than $Pt_{1ML}Ni$ (one monolayer of the Pt shell on a Ni core) and $Pt_{1ML}Ni_4N$ (one monolayer of the Pt shell on a Ni_4N core). By adding one more layer of Pt in the shell, the effects of Ni and Ni_4N cores on the Pt shell are significantly decreased (Figure S7, Supporting Information). In addition, the surface contraction in the Pt shell is reduced by changing the core from Ni to Ni_4N, leading to an up-shifted Pt d-band center and the strengthened O−Pt interaction (BE-O, −3.83 eV for $Pt_{2ML}Ni$ and −3.94 eV for $Pt_{2ML}Ni_4N$). Yet, compared to pure Pt, a more contraction on the surface of $Pt_{2ML}Ni_4N$ is observed (surface strain; −3.19% for $Pt_{2ML}Ni_4N$ and −3.04%, for Pt, Figure.5), which leads the down-shifted d-band center of Pt (Figure S7, Supporting Information) and the weaker BE-O (BE-O; −3.94 eV for $Pt_{2ML}Ni_4N$ and −4.09 eV for Pt, Figure 5a). Therefore, our DFT results clearly support the experimental finding of the higher ORR activity of PtNiN than Pt (Figure 5b). As reported,[8] too much introduction of Ni into the core leads to the instability of the nanoparticles due to too highly strained surface (Figure S7 and Table S1, Supporting Information). It may be evident that the Ni_3N phase is negligibly found in the X-ray spectrum compared to the Ni_4N phase (Figure S2, Supporting Information). It is also well-known that PtNi core−shell electrocatalysts are not durable in acidic condition due to the significant Ni dissolution.[19,20]

Moreover, to gain the understanding of the enhanced durability of PtNiN/C, in this DFT study, similar to the previous one,[34] we took into account the unavoidable imperfection of the nanoparticles. It has been found that vacancies are more favorably formed at the vertex and edge sites than at terraces owing to their lower formation energies. Thus only the diffusion of Pt from a vertex of the inner shell to vacancy sites at the vertex of the outmost shell was considered. Using the $Pt_{2ML}Ni_4N$ model, our calculations show that the energy cost for the Pt diffusion depends on the existence of N atoms. For the inner Pt atom next to the N atom, it needs only 0.15 eV, while for those far away from the N atom the energy is 0.33 eV, which is consistent with that using $Pt_{2ML}Ni$ (0.37 eV). In contrast, pure Pt costs a much higher energy for the diffusion (0.42 eV). Therefore, our calculations suggest that $Pt_{2ML}Ni_4N$ has a higher stability than Pt by enabling the easier diffusion of Pt from inner shells to surfaces filling the defect sites and thus preventing the dissolution of Pt into the electrolyte. Accordingly, a higher N concentration may facilitate the Pt diffusion and therefore, increase the durability. To further examine this effect, one more N atom was added at the interface between the Pt shell and the Ni_4N core, assuming the

dx.doi.org/10.1021/nl303362s | Nano Lett. 2012, 12, 6266−6271

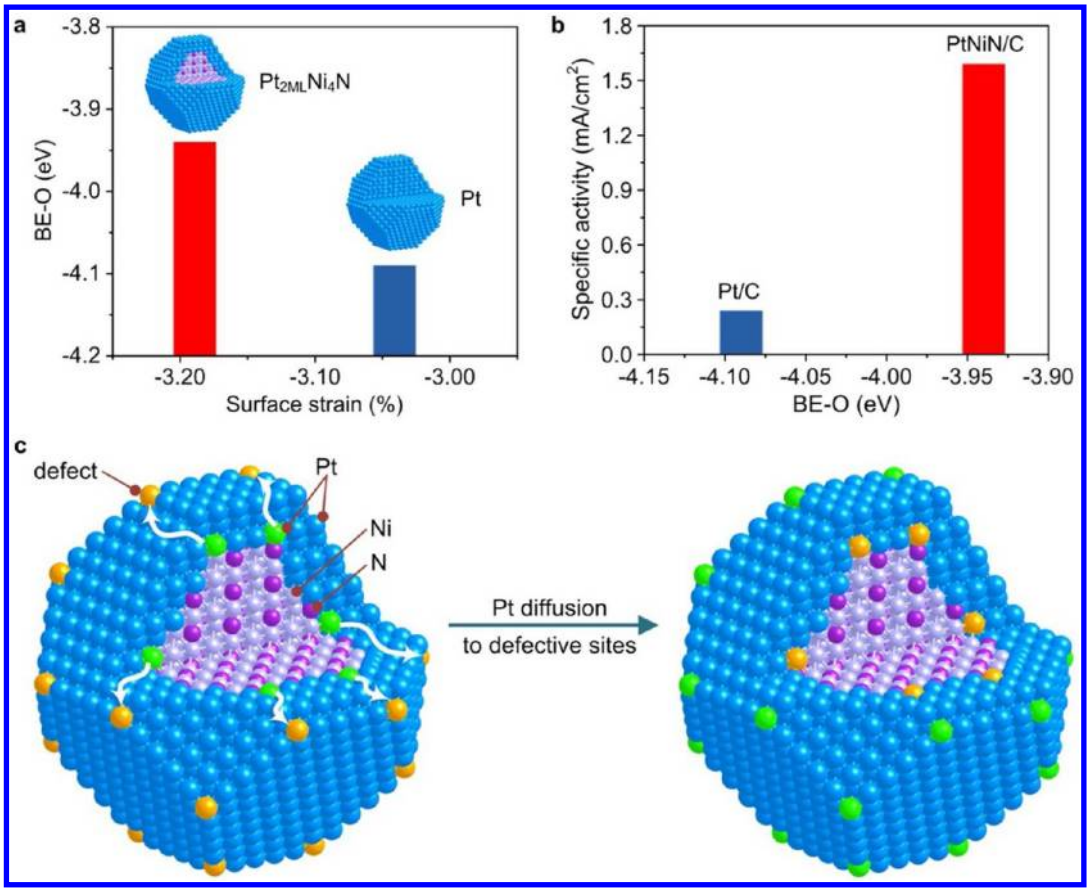

Figure 5. (a) Comparison of surface strain versus predicted binding energy of oxygen (BE-O) on the $Pt_{2\ ML}Ni_4N$ and Pt nanoparticle models with ~1.7 nm. The more negative strain corresponds to further compression. To predict the BE-Os, an atomic oxygen was placed at a fcc active site on the (111) plane. (b) Pt specific activity against BE-O on PtNiN/C and Pt/C. (c) Schematic of the inner Pt diffusion process to the defective sites at the vertex during cycling in the electrolyte. For clarity, the inner Pt atoms involved in diffusion are described in green, while the defects in yellow.

presence of a localized Ni_3N, as shown in Figure S2, Supporting Information. By interacting with one more N atom, the energy cost for the inner Pt atom to diffuse to the vacancy site on the surface is decreased from 0.15 to 0.10 eV, affirming the concentration of N is crucial to the durability of the catalysts. Overall, using Ni nitrides as the core enhances the ORR activity and durability via both geometric and electronic effects. The nitriding of the Ni core tunes the electronic structure of the Pt shell to display a higher ORR activity than Pt (electronic effect). Simultaneously, the presence of N atoms in the core allows a facile diffusion of interacted Pt from inner shells to the surface filling the vacancy sites (geometric effect), resulting in augmented durability of the catalysts.

In conclusion, we have reported on a new promising route to the development of novel core−shell catalysts with substantial reduction in Pt loading while retaining high ORR activity and stability. Using aberration-corrected STEM-HAADF and EELS mapping techniques we have investigated the core−shell structure of the catalyst which are stable against corrosion during ORR. Electrochemistry and DFT methods reveal that the high ORR activity and durability of PtNiN catalyst is attributed to Ni nitride core, modifying the behavior of Pt shell by inducing both geometric and electronic effects. These advances also open up broad possibilities for the design and synthesis of various transition metal nitride based core−shell nanoparticles for a wide range of applications in energy conversion processes.

■ ASSOCIATED CONTENT

Supporting Information

Materials and Method section describing all experimental procedures, additional STEM-EELS data, and in *situ* XANES and XRD data along with DFT calculated parameters. This material is available free of charge via the Internet at http://pubs.acs.org.

■ AUTHOR INFORMATION

Corresponding Author

*E-mail: adzic@bnl.gov. Telephone: (+1-631) 3444522. Fax: (+1-631) 3445815.

Author Contributions

The manuscript was written through contributions of all authors. All authors have given approval to the final version of the manuscript.

Notes

The authors declare no competing financial interest.

■ ACKNOWLEDGMENTS

This research was performed at Brookhaven National laboratory under contract DE-AC02-98CH10886 with the US Department of Energy, Division of Chemical Sciences, Geosciences and Biosciences Division. We thank the National Energy Research Scientific Computing Center (NERSC), which is supported by the Office of Science of the U.S. DOE under Contract No. DE-AC02-05CH11231 and BNL's Center

for Functional Nanomaterials (CFN) for computational time. Work at the NSLS was supported by the DOE BES Grant DE-FG02-03ER15688.

REFERENCES

(1) Steele, B. C. H.; Heinzel, A. *Nature* **2001**, *414* (6861), 345−352.
(2) Vielstich, W.; Lamm, A.; Gasteiger, H. A., *Handbook of Fuel Cells − Fundamentals, Technology and Applications*. John Wiley & Sons: Chichester, U.K., 2003.
(3) Yeager, E. *Electrochim. Acta* **1984**, *29* (11), 1527−1537.
(4) Gasteiger, H. A.; Kocha, S. S.; Sompalli, B.; Wagner, F. T. *Appl. Catal. B: Environ.* **2005**, *56* (1−2), 9−35.
(5) Adzic, R. R., *Frontiers in Electrochemistry*. VCH Publishers: New York, 1998; Vol. *5*.
(6) Mukerjee, S.; Srinivasan, S. *J. Electroanal. Chem.* **1993**, *357* (1−2), 201−224.
(7) Toda, T.; Igarashi, H.; Uchida, H.; Watanabe, M. *J. Electrochem. Soc.* **1999**, *146* (10), 3750−3756.
(8) Kuttiyiel, K. A.; Sasaki, K.; Choi, Y.; Su, D.; Liu, P.; Adzic, R. R. *Energ. Environ. Sci.* **2012**, *5* (1), 5297−5304.
(9) Sasaki, K.; Naohara, H.; Cai, Y.; Choi, Y. M.; Liu, P.; Vukmirovic, M. B.; Wang, J. X.; Adzic, R. R. *Angew. Chem., Int. Ed.* **2010**, *49* (46), 8602−8607.
(10) Lima, F. H. B.; Zhang, J.; Shao, M. H.; Sasaki, K.; Vukmirovic, M. B.; Ticianelli, E. A.; Adzic, R. R. *J. Phys. Chem. C* **2007**, *111* (1), 404−410.
(11) Mani, P.; Srivastava, R.; Strasser, P. *J. Power Sources* **2011**, *196* (2), 666−673.
(12) Strasser, P.; Koh, S.; Anniyev, T.; Greeley, J.; More, K.; Yu, C. F.; Liu, Z. C.; Kaya, S.; Nordlund, D.; Ogasawara, H.; Toney, M. F.; Nilsson, A. *Nat. Chem.* **2010**, *2* (6), 454−460.
(13) Liu, G. C. K.; Stevens, D. A.; Burns, J. C.; Sanderson, R. J.; Vernstrom, G.; Atanasoski, R. T.; Debe, M. K.; Dahn, J. R. *J. Electrochem. Soc.* **2011**, *158* (8), B919−B926.
(14) Morozan, A.; Jousselme, B.; Palacin, S. *Energ. Environ. Sci.* **2011**, *4* (4), 1238−1254.
(15) Yang, H. *Angew. Chem., Int. Ed.* **2011**, *50* (12), 2674−2676.
(16) Zhang, J.; Yang, H. Z.; Fang, J. Y.; Zou, S. Z. *Nano Lett.* **2010**, *10* (2), 638−644.
(17) Stamenkovic, V. R.; Fowler, B.; Mun, B. S.; Wang, G. F.; Ross, P. N.; Lucas, C. A.; Markovic, N. M. *Science* **2007**, *315* (5811), 493−497.
(18) Wu, J. B.; Zhang, J. L.; Peng, Z. M.; Yang, S. C.; Wagner, F. T.; Yang, H. *J. Am. Chem. Soc.* **2010**, *132* (14), 4984−4985.
(19) Wang, C.; Chi, M. F.; Wang, G. F.; van der Vliet, D.; Li, D. G.; More, K.; Wang, H. H.; Schlueter, J. A.; Markovic, N. M.; Stamenkovic, V. R. *Adv. Funct. Mater.* **2011**, *21* (1), 147−152.
(20) Travitsky, N.; Ripenbein, T.; Golodnitsky, D.; Rosenberg, Y.; Burshtein, L.; Peled, E. *J. Power Sources* **2006**, *161* (2), 782−789.
(21) Tao, F.; Grass, M. E.; Zhang, Y. W.; Butcher, D. R.; Renzas, J. R.; Liu, Z.; Chung, J. Y.; Mun, B. S.; Salmeron, M.; Somorjai, G. A. *Science* **2008**, *322* (5903), 932−934.
(22) Sasaki, K.; Kuttiyiel, K. A.; Barrio, L.; Su, D.; Frenkel, A. I.; Marinkovic, N.; Mahajan, D.; Adzic, R. R. *J. Phys. Chem. C* **2011**, *115* (20), 9894−9902.
(23) Alayoglu, S.; Nilekar, A. U.; Mavrikakis, M.; Eichhorn, B. *Nat. Mater.* **2008**, *7* (4), 333−338.
(24) Yan, J. M.; Zhang, X. B.; Akita, T.; Haruta, M.; Xu, Q. *J. Am. Chem. Soc.* **2010**, *132* (15), 5326−+.
(25) Miura, A.; Tague, M. E.; Gregoire, J. M.; Wen, X. D.; van Dover, R. B.; Abruna, H. D.; DiSalvo, F. J. *Chem. Mater.* **2010**, *22* (11), 3451−3456.
(26) Zhong, H. X.; Zhang, H. M.; Liu, G.; Liang, Y. M.; Hu, J. W.; Yi, B. L. *Electrochem. Commun.* **2006**, *8* (5), 707−712.
(27) Swanson, H. E.; Tatge, E. *Natl. Bur. Stand. (U.S.), Circ.* **1953**, *13*, 539.
(28) Juza, R.; Sachze, W. *Z. Anorg. Allg. Chem.* **1943**, *251* (2), 201−212.
(29) Neklyudov, I. M.; Morozov, A. N. *Physica B* **2004**, *350* (4), 325−337.
(30) Belii, I. M.; Komarov, F. F.; Tishkov, V. S.; Yankovskii, V. M. *Phys. Stat. Solidi A: Appl. Res.* **1978**, *45* (1), 343−352.
(31) Schmidt, T. J.; Gasteiger, H. A.; Stab, G. D.; Urban, P. M.; Kolb, D. M.; Behm, R. J. *J. Electrochem. Soc.* **1998**, *145* (7), 2354−2358.
(32) Zhang, J.; Sasaki, K.; Sutter, E.; Adzic, R. R. *Science* **2007**, *315* (5809), 220−222.
(33) Greeley, J.; Stephens, I. E. L.; Bondarenko, A. S.; Johansson, T. P.; Hansen, H. A.; Jaramillo, T. F.; Rossmeisl, J.; Chorkendorff, I.; Norskov, J. K. *Nat. Chem.* **2009**, *1* (7), 552−556.
(34) Sasaki, K.; Naohara, H.; Choi, Y.; Cai, Y.; Chen, W. F.; Liu, P.; Adzic, R. *Nat. Commun.* **2012**, *3*, 1115.